

Polydopamine-Coated Solid Silica Nanoparticles Encapsulating IR-783 Dyes: Synthesis and NIR Fluorescent Cell Imaging

Yoshio Nakahara,* Haruki Nakabayashi, Jun Miyazaki, Mitsuru Watanabe, Toshiyuki Tamai, and Setsuko Yajima



Cite This: *ACS Omega* 2024, 9, 19932–19939



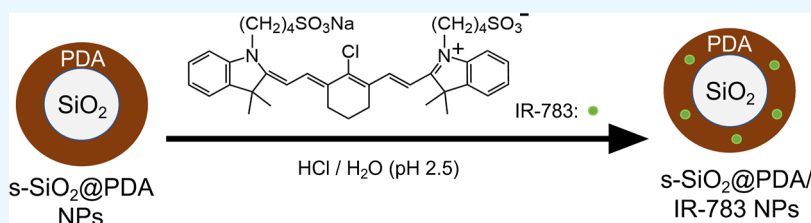
Read Online

ACCESS |

Metrics & More

Article Recommendations

Supporting Information



ABSTRACT: We report a simple and efficient synthetic method for polydopamine (PDA)-coated solid silica nanoparticles ($s\text{-SiO}_2\text{@PDA}$ NPs) encapsulating anionic near-infrared (NIR) fluorescent dyes through physical adsorption. Despite the use of anionic NIR fluorescent dyes indocyanine green (ICG) and 2-[2-[2-chloro-3-[2-[1,3-dihydro-3,3-dimethyl-1-(4-sulfobutyl)-2H-indol-2-ylidene]-ethylidene]-1-cyclohexen-1-yl]-ethenyl]-3,3-dimethyl-1-(4-sulfobutyl)-3H-indolium (IR-783), they were successfully immobilized on anionic $s\text{-SiO}_2\text{@PDA}$ NP surfaces under acidic aqueous conditions. After embedding in the $s\text{-SiO}_2\text{@PDA}$ NPs, the fluorescence of ICG was almost quenched, while a diminished IR-783 fluorescence remained observable. The fluorescence intensity of IR-783 embedded in $s\text{-SiO}_2\text{@PDA}$ NPs remained almost constant over 2 weeks in a pseudobiological solution, with a slight reduction due to dye degradation and dye leakage from the $s\text{-SiO}_2\text{@PDA}$ NPs. Finally, the $s\text{-SiO}_2\text{@PDA}$ NPs encapsulating IR-783 were successfully used for NIR fluorescent imaging of African green monkey kidney cells.

INTRODUCTION

In recent years, a variety of nanoparticles (NPs) have been developed for medical purposes. For example, magnetic NPs have been prepared for drug delivery and magnetic resonance imaging.^{1–3} Among them, near-infrared (NIR) fluorescent NPs have attracted enormous interest because they enable us to observe biological phenomena in situ directly, benefiting from the deep penetration of tissue by NIR fluorescence.⁴ NIR-fluorescent-dye-doped silica nanoparticles (SiO_2 NPs) are particularly viable nanoprobess^{5–10} for their optimal fluorescence bioimaging properties, including better biocompatibility, higher hydrophilicity, and excellent size control, compared with heavy metal quantum dots.¹¹ Chemical modification and physical adsorption are the two primary approaches for NIR fluorescent dye immobilization in SiO_2 NPs. Chemical modification is often used to conjugate fluorescent organic dyes to SiO_2 NPs via chemical bonds due to greater dye encapsulation stability.¹² However, chemical modification is limited to some reactive dyes, which are often expensive and scarce. Additionally, many NIR fluorescent dyes are extremely susceptible to heat and alkaline conditions and are often required for chemical conjugation processes. However, physical adsorption allows the use of a wide range of dyes with mild synthetic conditions, as a chemical reaction is not required for dye immobilization. Therefore, an approach

enabling the efficient incorporation of NIR fluorescent dyes into SiO_2 NPs through physical adsorption is desirable.

Polydopamine (PDA) is a mussel-inspired biopolymer obtained by the oxidative polymerization of dopamine under mild alkaline conditions.¹³ PDA can be deposited on almost any NP surface^{14,15} with PDA-coated NPs yielding good biocompatibility in the human body.¹⁶ The deposited PDA layer allows easy and rapid modification with functional ligands through Schiff base reactions and/or Michael addition even on the NP surface.¹⁷ For example, PDA-coated NPs were chemically modified with polyethylene glycol to enhance their colloidal characteristics.^{18,19} Additionally, planar aromatic compounds such as doxorubicin and methylene blue can be loaded in the PDA layer, facilitated by hydrophobic interactions and $\pi\text{-}\pi$ stacking.^{20,21} Indocyanine green (ICG), a representative NIR fluorescent dye, is also physically encapsulated into PDA-coated NPs.^{22,23} ICG is a FDA-approved NIR fluorescent dye used in bioimaging for medical

Received: December 3, 2023

Revised: April 7, 2024

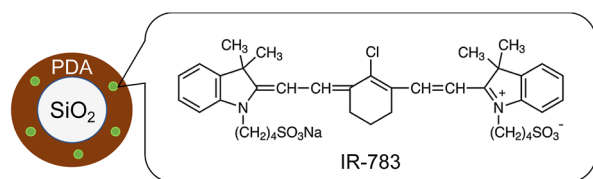
Accepted: April 10, 2024

Published: April 24, 2024



diagnosis (FDA, U.S. Food and Drug Administration),²⁴ but this dye incorporates poorly into SiO₂ NPs using conventional methods due to strong electrostatic repulsion between sulfonates of ICG and silanol groups of SiO₂ NPs.²⁵ However, ICG loading of PDA-coated mesoporous SiO₂ NPs (*m*-SiO₂ NPs) is possible using room-temperature physical adsorption.²⁶ It may be that the porous structure of the *m*-SiO₂ NPs weakens the electrostatic repulsion. Although PDA-coated *m*-SiO₂ NPs are good candidates to incorporate anionic NIR fluorescent dyes, solid SiO₂ NPs (*s*-SiO₂ NPs) are better substrates for their excellent size control and wide availability.

In this study, we designed a new fabrication strategy for PDA-coated *s*-SiO₂ NPs encapsulating anionic NIR fluorescent dyes using room-temperature physical adsorption and then examined their fluorescence and colloidal properties in water to evaluate performance as fluorescence bioimaging agents. The schematic illustration of the target NP is shown in Figure 1. As an anionic NIR fluorescent dye, 2-[2-[2-chloro-3-[2-[1,3-



s-SiO₂@PDA/IR-783 NPs

Figure 1. Schematic illustration of the *s*-SiO₂@PDA/IR-783 NPs.

dihydro-3,3-dimethyl-1-(4-sulfobutyl)-2*H*-indol-2-ylidene]-ethylidene]-1-cyclohexen-1-yl]-ethenyl]-3,3-dimethyl-1-(4-sulfobutyl)-3*H*-indolium (IR-783) was selected instead of ICG since ICG undergoes strong fluorescence quenching in PDA-coated NPs.²³ Additionally, IR-783 has excellent biocompatibility, high extinction coefficient, and high photochemical stability compared with other commercially available NIR fluorescent dyes.^{27,28} Despite the ease in incorporating anionic NIR fluorescent dyes into cationic NPs due to electrostatic interactions, cationic NPs are frequently associated with adverse health effects in animal studies.²⁹ Cationic dyes are also undesirable as fluorescence bioimaging agents for similar reasons. Therefore, we aimed at anionic NIR fluorescent dye immobilization into anionic *s*-SiO₂ NPs using physical adsorption other than electrostatic interactions. First, *s*-SiO₂ NPs with a diameter of 50 nm were coated with PDA under mild alkaline conditions at room temperature (*s*-SiO₂@PDA NPs). Next, IR-783 was incorporated into the PDA layer of *s*-SiO₂@PDA NPs under acidic aqueous conditions at room temperature using hydrophobic interactions and π - π stacking (*s*-SiO₂@PDA/IR-783 NPs). We have found no reports of successful anionic NIR fluorescent dye immobilization on *s*-SiO₂ surfaces using physical adsorption. After NP characterization and property evaluation, the *s*-SiO₂@PDA/IR-783 NPs were then used for the fluorescence imaging of African green monkey kidney cells (COS-7).

RESULTS AND DISCUSSION

Synthesis and Characterization of *s*-SiO₂@PDA/IR-783 NPs. The synthesis of *s*-SiO₂@PDA/IR-783 NPs is shown in Figure 2. The *s*-SiO₂@PDA NP process uses the typical PDA coating method for NPs.¹⁹ In this study, commercially available spherical 50 nm diameter *s*-SiO₂ NPs were used as the core NPs. The specific surface area of the *s*-SiO₂ NPs was

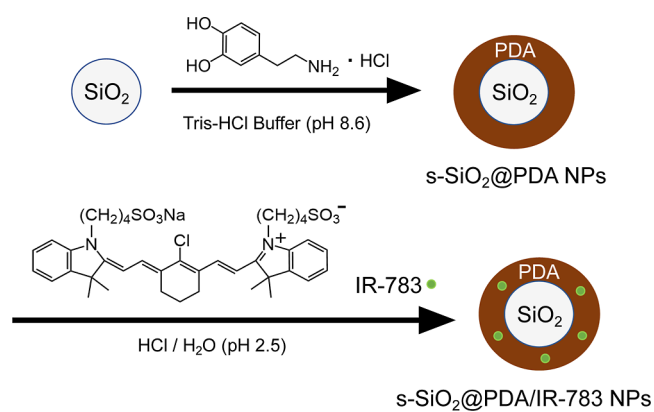


Figure 2. Synthesis of the *s*-SiO₂@PDA/IR-783 NPs.

76 m² g⁻¹, which was determined by BET measurements. It means that *s*-SiO₂ NPs are standard solid NPs.³⁰ Before the PDA coating, *s*-SiO₂ NPs were dispersed in 50 mM Tris-HCl buffer aqueous solution (pH 8.6). When dopamine hydrochloride was added to the *s*-SiO₂ NP aqueous solution, the reaction mixture immediately changed from colorless to dark brown. The mixture was stirred continuously at room temperature for 18 h. After the reaction had reached completion, *s*-SiO₂@PDA NPs were isolated by centrifugation. Organic compound content before and after PDA coating was evaluated by thermogravimetric analysis (TGA) (Figure S1). TGA was performed under a helium atmosphere at a rate of 10 °C min⁻¹ in the temperature range from 25 to 500 °C. In both cases, the weight loss (ca. 2.5 wt %) from 25 to 100 °C is originated from the removal of water adsorbed on the NPs. The total weight loss (6.4 wt %) of *s*-SiO₂@PDA NPs increased by 2 wt % compared with that (4.4 wt %) of *s*-SiO₂ NPs. This evidence supports the presence of a PDA coating on the *s*-SiO₂ NP surface.

Next, under dark conditions, *s*-SiO₂@PDA NPs were redispersed in an aqueous HCl solution (pH 2.5) containing IR-783. The mixture was stirred continuously at room temperature for 24 h. After purification by centrifugation, isolated *s*-SiO₂@PDA/IR-783 NPs were redispersed in Milli-Q water. For comparison, IR-783 incorporation was also performed in Milli-Q water (pH ca. 6). Figure 3 shows the extinction spectra of *s*-SiO₂@PDA/IR-783 NPs, which were prepared in HCl aqueous solution and in Milli-Q water, dispersed in Milli-Q water. The extinction for NPs prepared in HCl aqueous solution was much higher than that of NPs prepared in Milli-Q water. This demonstrates that IR-783 is

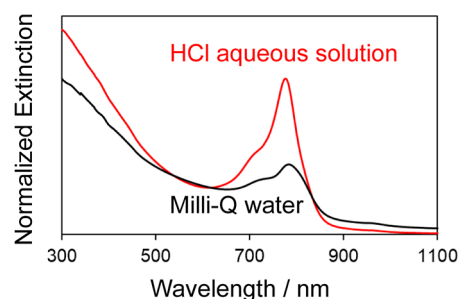


Figure 3. Extinction spectra of *s*-SiO₂@PDA/IR-783 NPs, which were prepared in HCl aqueous solution and in Milli-Q water, dispersed in Milli-Q water.

incorporated more easily under acidic aqueous conditions than in neutral aqueous conditions. Under acidic aqueous conditions, the electrostatic repulsion between silanol groups of $s\text{-SiO}_2\text{@PDA}$ NPs and sulfonates of IR-783 may be weakened. In this regard, Mrowczynski et al. also reported the successful incorporation of ICG into PDA-coated carbon nanodiamonds in aqueous acidic conditions (pH 2.5).³¹ Fortunately, this experimental procedure was also applicable to the immobilization of IR-783 into $s\text{-SiO}_2\text{@PDA}$ NPs.

Figure 4 shows the transmission electron microscopy (TEM) images and particle size distributions of $s\text{-SiO}_2$ NPs,

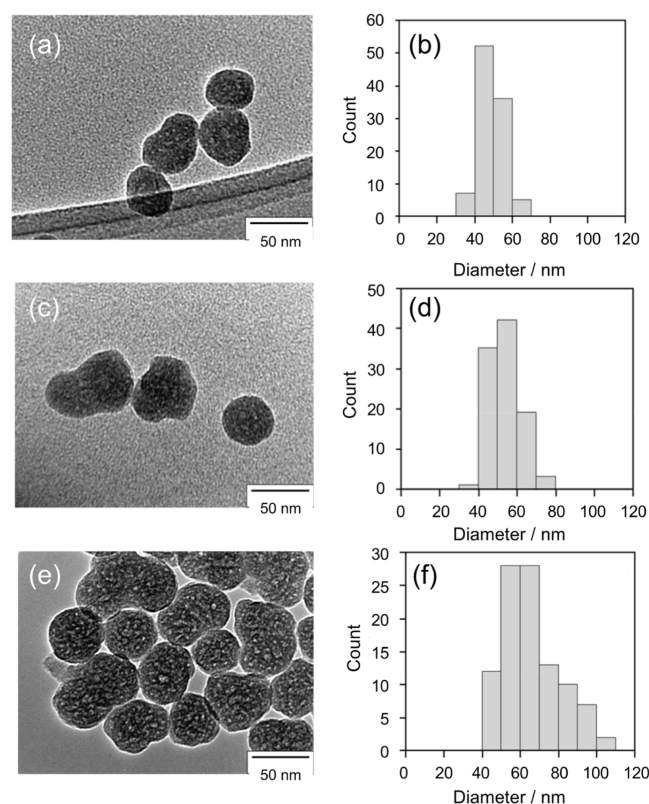


Figure 4. (a,c,e) TEM images and (b,d,f) particle size distributions of (a,b) $s\text{-SiO}_2$ NPs, (c,d) $s\text{-SiO}_2\text{@PDA}$ NPs, and (e,f) $s\text{-SiO}_2\text{@PDA/IR-783}$ NPs.

$s\text{-SiO}_2\text{@PDA}$ NPs, and $s\text{-SiO}_2\text{@PDA/IR-783}$ NPs. Analysis with the NIH ImageJ software³² yields average diameters for $s\text{-SiO}_2$ NPs, $s\text{-SiO}_2\text{@PDA}$ NPs, and $s\text{-SiO}_2\text{@PDA/IR-783}$ NPs of 49 ± 6 nm, 54 ± 8 nm, and 66 ± 15 nm, respectively. The average thickness of the PDA layer on $s\text{-SiO}_2$ NPs was estimated to be about 2.5 nm from TEM images. There was no significant difference in average diameter. Therefore, we judged that no aggregation was caused by the chemical modification performed in this study. The overall morphology of $s\text{-SiO}_2$ NPs was mostly unchanged before and after modification. The acidic aqueous conditions when loading IR-783 minimally impacted the $s\text{-SiO}_2$ NP morphology. Figure S2 shows the NP size distributions obtained by dynamic light scattering in Milli-Q water. Table S1 shows the NP average hydrodynamic diameter, polydispersity index, and zeta potentials of NPs when dispersed in Milli-Q water. The average hydrodynamic diameters of $s\text{-SiO}_2\text{@PDA}$ NPs and $s\text{-SiO}_2\text{@PDA/IR-783}$ NPs were slightly larger than that of $s\text{-SiO}_2$ NPs. These NPs are well dispersed in Milli-Q water and have zeta potentials

below -30 mV. According to DLVO theory, this zeta potential indicates sufficient electrostatic repulsion to improve colloidal stability for good dispersion in water.³³

Fluorescent Properties of $s\text{-SiO}_2\text{@PDA/IR-783}$ NPs in Aqueous Solution. Figure S3 shows the fluorescence spectra of $s\text{-SiO}_2\text{@PDA/IR-783}$ NPs and free IR-783 in Milli-Q water. Both spectra are almost identical, indicating that the IR-783 fluorescence is unchanged after the 24 h immersion in acidic aqueous conditions. The incorporation ratio of IR-783 in $s\text{-SiO}_2\text{@PDA}$ NPs was quantified by dividing the amount of incorporated IR-783, determined based on absorbance at 750 nm, from the initially added amount of IR-783.³⁴ The incorporation ratio of IR-783 in $s\text{-SiO}_2\text{@PDA}$ NPs was determined to be 0.37. The loading amount of IR-783 to NPs was calculated to be 4.9×10^{-5} mol g^{-1} . Despite the negative charge on both the dye and NP surface, the incorporation ratio was comparatively high. As $s\text{-SiO}_2\text{@PDA/IR-783}$ NPs were washed by centrifugation three times, any adsorbed IR-783 on the NP surface through only van der Waals interaction must be removed. Therefore, IR-783 must be incorporated into the PDA layer via hydrophobic interactions and $\pi\text{-}\pi$ stacking like ICG.

Figure 5 shows the fluorescence and extinction spectra of $s\text{-SiO}_2\text{@PDA/IR-783}$ and $s\text{-SiO}_2\text{@PDA/ICG}$ NPs dispersed in Milli-Q water. From the extinction spectra, ICG is incorporated into $s\text{-SiO}_2\text{@PDA}$ NPs. However, the fluorescence of $s\text{-SiO}_2\text{@PDA/ICG}$ NP was significantly different from that of free ICG (Figure S4) and was almost quenched in an aqueous solution. This observation is consistent with other reports^{23,26} and results from ICG self-aggregation.³⁵ Interestingly, the fluorescence of $s\text{-SiO}_2\text{@PDA/IR-783}$ NPs was significantly observed, although the quantum yield (2.2%) of $\text{SiO}_2\text{@PDA/IR-783}$ NPs was lower than that (3.7%) of IR-783. IR-783 is a cyanine dye with a rigid cyclohexenyl substitution introduced in the middle of a polymethine linker and is unlikely to accumulate in normal cells.³⁶ It may be that IR-783 self-aggregation in the PDA layer is weaker than ICG self-aggregation due to its rigidity, and the decreased quantum yield of IR-783 is due to this moderate aggregation.

Time-Dependent Changes of Spectroscopic Properties of $s\text{-SiO}_2\text{@PDA/IR-783}$ NPs. In this section, time-dependent spectroscopic changes of $s\text{-SiO}_2\text{@PDA/IR-783}$ NPs were investigated because the dyes physically immobilized in the PDA layer are gradually released from the NP surface.³⁷ After the aqueous dispersions of $s\text{-SiO}_2\text{@PDA/IR-783}$ NPs were prepared, they were stored under ambient conditions in the dark at room temperature. Figure 6 shows the time-course change in the relative fluorescence intensity of $\text{SiO}_2\text{@PDA/IR-783}$ NPs dispersed in Milli-Q water. Here, the NP fluorescence intensity immediately after preparation was assigned as 100, and data were normalized to this. The fluorescence intensity undergoes a rapid decrease within the first few hours. This may be a burst-release phenomenon of dyes from the NPs to bulk water,³⁸ which increases the nonradiative deactivation based on the movement of released dyes.⁹ Subsequently, the fluorescence of the $s\text{-SiO}_2\text{@PDA/IR-783}$ NPs gradually increases. This may be attributed to reduced aggregation of the dyes released from the NPs into the bulk water, which then reduces aggregation-induced fluorescence quenching. To investigate the relationship between release and fluorescence intensity, the extinction and fluorescence spectra of $\text{SiO}_2\text{@PDA/IR-783}$ NPs were measured in aqueous solutions prepared at different pHs, which were adjusted by citric acid

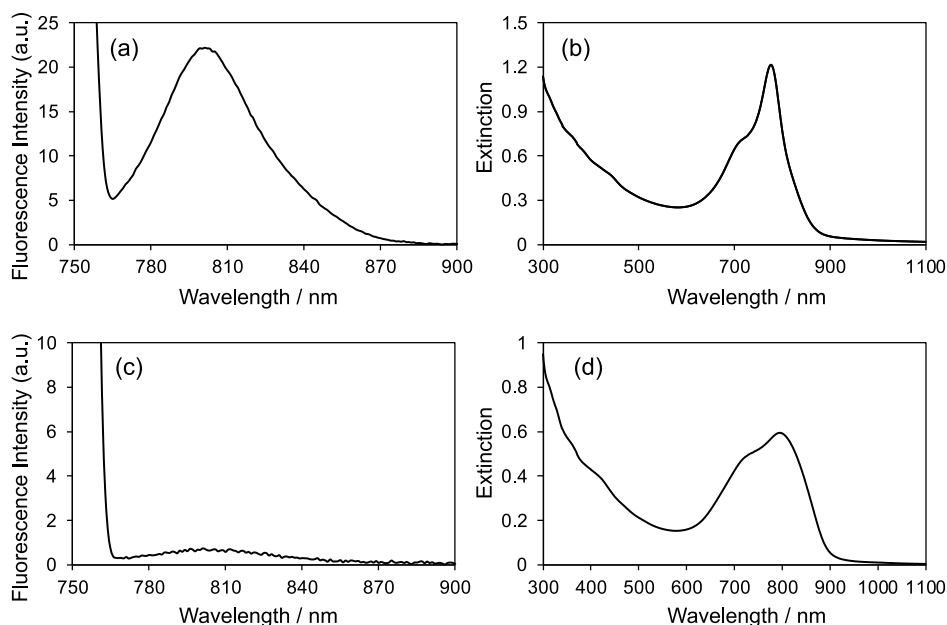


Figure 5. (a,c) Fluorescence spectra and (b,d) extinction spectra of (a,b) s-SiO₂@PDA/IR-783 NPs ($\lambda_{\text{ex}} = 750$ nm) and (c), (d) s-SiO₂@PDA/ICG NPs dispersed in Milli-Q water ($\lambda_{\text{ex}} = 750$ nm).

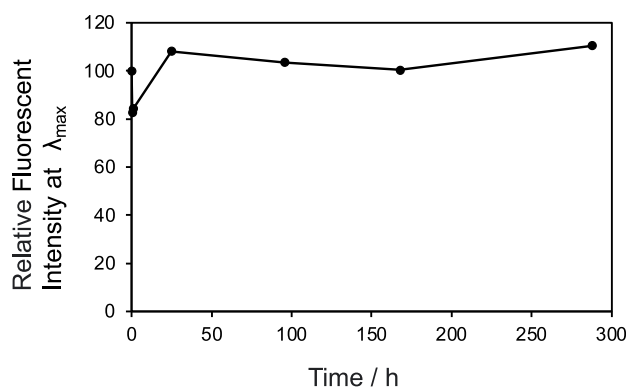


Figure 6. Time-course change in the relative fluorescence intensity of s-SiO₂@PDA/IR-783 NPs dispersed in Milli-Q water ($\lambda_{\text{ex}} = 750$ nm).

(Figure 7). An optical response by a pH change is expected for the following phenomenon. In the PDA layer, phenol proton dissociation is increased at higher pHs. As deprotonated phenol groups are negatively charged, they electrostatically repel anionic IR-783, promoting dye release from the NPs. The fluorescence intensity of SiO₂@PDA/IR-783 NPs increased with pH increase, yet the extinction remained almost unchanged over all pHs evaluated. Thus, while some dyes were released from the NPs at higher pHs, the corresponding disruption of IR-783 aggregates in bulk water restored the fluorescence intensity. Therefore, it is concluded that the release of dyes from NPs increases the fluorescence intensity.

Generally, NIR fluorescent dyes are susceptible to degradation in water. ICG is reported to undergo a 65.73% reduction in fluorescence intensity after 1 day.³⁹ Figure S5 shows the time-course changes in the relative extinction of SiO₂@PDA/IR-783 NPs and free IR-783 dispersed in Milli-Q water. Here, the measured extinction immediately after preparation was assigned as 100, and data were normalized to this. In both cases, the extinction of IR-783 remained >60% of the initial value after 12 days. The inherent stability of IR-783 originates from the different chemical structures of the

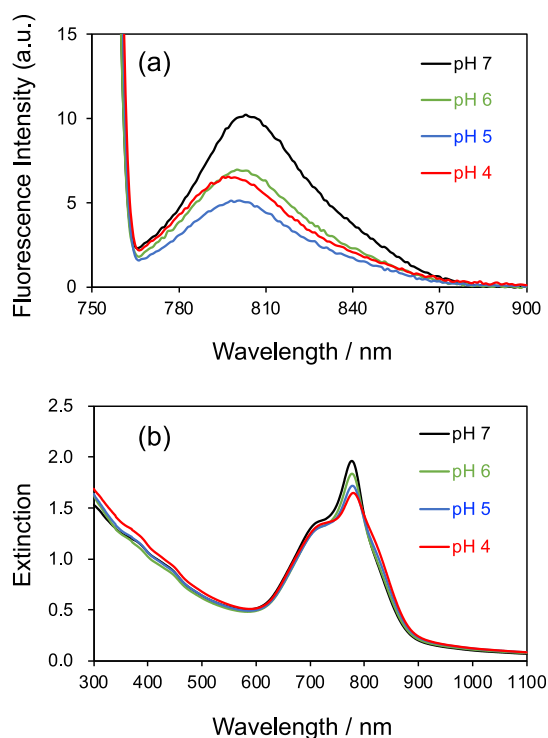


Figure 7. (a) Fluorescence and (b) extinction spectra of s-SiO₂@PDA/IR-783 NPs dispersed in aqueous solutions prepared at different pH values ($\lambda_{\text{ex}} = 750$ nm).

linker moiety from ICG. Additionally, IR-783 incorporated in the NPs decomposed a bit more slowly than free IR-783. This stability improvement may be due to the movement restriction of dyes in the PDA layer.

Figure 8 shows the proposed behavior of SiO₂@PDA/IR-783 NPs dispersed in water based on the obtained experimental results. Under acidic aqueous conditions, IR-783 is incorporated in the PDA layer via hydrophobic interactions and π - π stacking. Within this layer, the dyes are

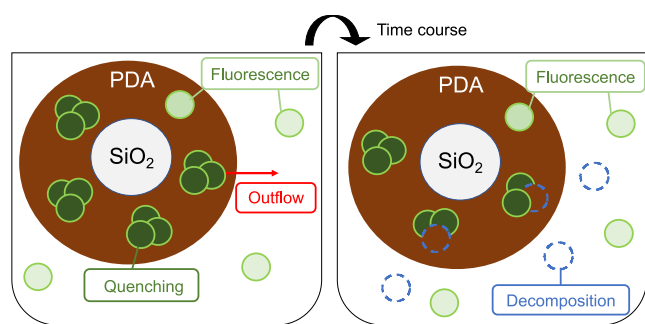


Figure 8. Plausible behavior of $s\text{-SiO}_2\text{@PDA/IR-783}$ NPs dispersed in water.

moderately aggregated, which diminishes the fluorescence. Upon dispersal of $\text{SiO}_2\text{@PDA/IR-783}$ NPs in fresh Milli-Q water, aggregated IR-783 is released from the NPs into the bulk water as a function of concentration. Aggregated IR-783 then gradually deaggregates in the bulk water, restoring the fluorescence of IR-783. Counter to this, IR-783 in solution undergoes slow decomposition, reducing the fluorescence intensity. These positive and negative factors both affect the $\text{SiO}_2\text{@PDA/IR-783}$ NPs fluorescence, resulting in an essentially constant intensity for 12 days.

Behavior of $s\text{-SiO}_2\text{@PDA/IR-783}$ NPs in a Biological Environment. Before NIR fluorescent bioimaging, $s\text{-SiO}_2\text{@PDA/IR-783}$ NPs were dispersed in 50 mM Tris-HCl buffer aqueous solution (pH 7.4) containing 150 mM NaCl as a pseudobiological solution and stored in the dark. After 2 weeks, no significant aggregate was observed in the solution, and the fluorescence spectrum was measured. Figure 9 shows

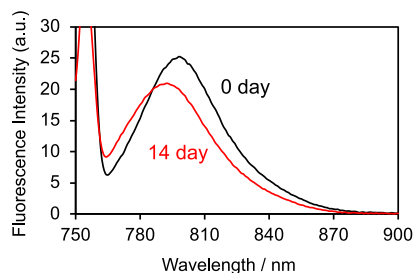


Figure 9. Fluorescence spectra and time-course changes of $s\text{-SiO}_2\text{@PDA/IR-783}$ NPs dispersed in 50 mM Tris-HCl buffer aqueous solution (pH 7.4) containing 150 mM NaCl ($\lambda_{\text{ex}} = 750$ nm).

the fluorescence spectra and time-course changes of the solution. After 2 weeks, the fluorescence intensity was about 80% of the initial intensity. This supports the viability of $s\text{-SiO}_2\text{@PDA/IR-783}$ NPs as bioimaging agents.

Next, $s\text{-SiO}_2\text{@PDA/IR-783}$ NPs were introduced into the COS-7 cells (originally isolated from African green monkey kidney, RIKEN BRC RCB0539) by lipofectamine 2000, a cationic lipid transfection reagent.⁴⁰ The $s\text{-SiO}_2\text{@PDA/IR-783}$ NP aqueous solution (0.15 mg mL^{-1}) was mixed with the same volume of the original lipofectamine 2000 solution, with the cationic lipofectamine 2000 adsorbing to the negatively charged NP surface.^{10,41} This adsorption changes the surface charge of the $s\text{-SiO}_2\text{@PDA/IR-783}$ NPs from anionic to cationic. These positively charged NPs are then generally easier to be introduced into negatively charged cells.^{42,43} After the cellular uptake of NPs, cell imaging by a confocal fluorescence microscope was conducted. As a control, the same

experimental condition was performed but using free IR-783. Figure 10 shows bright-field and fluorescence images of the

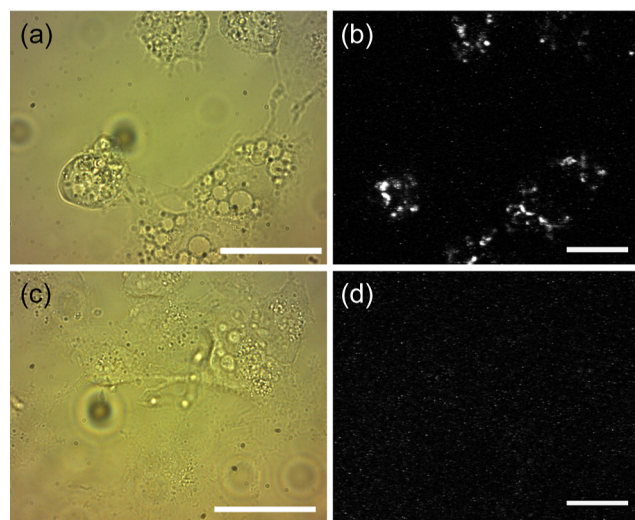


Figure 10. Bright-field images of COS-7 cells in the presence of (a) $\text{SiO}_2\text{@PDA/IR-783}$ NPs and (c) free IR-783. Fluorescence images of COS-7 cells in the presence of (b) $s\text{-SiO}_2\text{@PDA/IR-783}$ and (d) free IR-783 under dark conditions. Scale bar: 20 μm .

COS-7 cells. The excitation wavelength was 685 nm, and the fluorescence at wavelengths >700 nm was integrated and digitized. IR-783 can be finely excited at 685 nm (Figure S6). In the fluorescence images, the color intensity represents the integrated fluorescence intensity. As shown in Figure 10b, the fluorescence intensity of $\text{SiO}_2\text{@PDA/IR-783}$ NPs is stronger than that observed in Figure 10d. The faint white color observed over the whole area of Figure 10d may be due to excitation light source interference or excessive background adjustment during image processing. For quantitative analysis, the fluorescence intensity per cell area in Figure 10b–d was compared (Figure S7). As a result of the Welch t -test, the difference was considered statistically significant ($p = 0.017$). These results indicate that $s\text{-SiO}_2\text{@PDA/IR-783}$ NPs were successfully taken up into COS-7 cells via endocytosis and emitted detectable NIR fluorescence under biological conditions.

CONCLUSIONS

A novel NIR fluorescent bioimaging agent, $\text{SiO}_2\text{@PDA/IR-783}$ NPs, was fabricated by PDA coating and the subsequent incorporation of IR-783 under acidic aqueous conditions. The IR-783 fluorescent properties were unchanged even after immersion in acidic aqueous conditions. Interestingly, despite the fact that IR-783 is an anionic NIR fluorescent dye, it was easily incorporated into the anionic surface of $\text{SiO}_2\text{@PDA}$ NPs through physical adsorption. As chemical modification of cyanine dyes is difficult, this method poses an efficient preparation route to incorporate anionic cyanine dyes into anionic NP surfaces. Additionally, the PDA coating allows further NP functionalization, which may include targeting compounds to enable site-selective bioimaging. This study will be presented in future work.

■ EXPERIMENTAL SECTION

Chemicals. All chemicals and solvents were obtained commercially and used without further purification. Dulbecco's modified Eagle's medium and citric acid were purchased from FUJIFILM Wako Pure Chemical Corporation. Dopamine hydrochloride and ICG were obtained from Tokyo Chemical Industries Co., Ltd. Tris(hydroxymethyl)aminomethane (Tris) and IR-783 were purchased from MP Biomedicals and Sigma-Aldrich, respectively. Spherical s-SiO₂ NPs with a diameter of 50 nm were kindly donated from Fuso Chemical Co., Ltd. (product name: PL3). The specific surface area of the s-SiO₂ NPs was 76 m² g⁻¹ (BET measurements), which was provided by the production company. Lipofectamine 2000 was obtained from Thermo Fisher. Milli-Q water (deionized water) was prepared in our laboratory using a Milli-Q system, with the resulting water having a conductivity of 18 M Ω cm⁻¹.

Characterization. TEM images were taken at 100 kV with a JEM-2100 (JEOL, Japan). NP size distributions were quantitatively analyzed from several TEM images by NIH ImageJ software. The size distribution and zeta potential of NPs in aqueous solution were recorded at room temperature (about 25 °C) using an ELS Z particle size analyzer (Otsuka Electronics, Japan). Size distribution was evaluated by dynamic light scattering, with the average hydrodynamic diameter calculated based on the correlation function (cumulant analysis). Fluorescence spectra were recorded at room temperature using an RF-5300PC spectrofluorophotometer (Shimadzu, Japan) with quartz cells of 1 cm optical path length. In all fluorescence measurements, ICG and IR-783 were excited at 750 nm. Absolute fluorescence quantum yields were evaluated at room temperature using a Quantaaurus-QY (Hamamatsu Photonics, Japan). UV-vis extinction spectra were measured at room temperature using a JASCO V-730 BIO UV/vis spectrophotometer (Jasco, Japan) with quartz cells with a 1 cm optical path length. TGA was conducted by a ThermoMass Photo (Rigaku, Japan).

Synthesis of s-SiO₂@PDA NPs. The synthesis of s-SiO₂@PDA NPs was conducted as previously reported.¹⁹ First, s-SiO₂ NPs (200 mg) were finely dispersed by ultrasonication in 50 mL of 50 mM Tris-HCl aqueous buffer solution (pH 8.6). Next, dopamine hydrochloride (40 mg) was added to the aqueous solution containing s-SiO₂ NPs while stirring. The mixture was stirred continuously at room temperature (about 25 °C) for 18 h. After reaction, s-SiO₂@PDA NPs were collected by centrifugation at 15 000 rpm for 10 min. After supernatant removal, about 10 mL of Milli-Q water was added to the residue. This procedure was repeated twice. Finally, s-SiO₂@PDA NPs were finely dispersed by ultrasonication in 20 mL of Milli-Q water.

Synthesis of s-SiO₂@PDA/IR-783 NPs. The synthesis of s-SiO₂@PDA/IR-783 NPs was performed as previously reported.³¹ First, 9.4 mL of Milli-Q water containing s-SiO₂@PDA NPs (50 mg) was added to a centrifugation tube, and they were collected by centrifugation at 15 000 rpm for 10 min. After supernatant removal, s-SiO₂@PDA NPs were finely dispersed by ultrasonication in 10 mL of an HCl aqueous solution (pH 2.5). Next, 10 mL of HCl aqueous solution (pH 2.5) containing IR-783 (5.0 mg) was added to the HCl aqueous solution containing s-SiO₂@PDA NPs. The mixture was stirred continuously at room temperature (about 25 °C) for 24 h under dark conditions. After the reaction, s-SiO₂@PDA/IR-783 NPs were collected by centrifugation at 15 000

rpm for 15 min. After supernatant removal, about 10 mL of Milli-Q water was added to the residue. This procedure was repeated twice. Finally, s-SiO₂@PDA/IR-783 NPs were finely dispersed by ultrasonication in 10 mL of Milli-Q water. s-SiO₂@PDA/ICG NPs were also prepared using a similar method.

Determination of Incorporation Ratio of IR-783 into s-SiO₂ NPs. The incorporation ratio of IR-783 into s-SiO₂ NPs was quantified as follows. First, a standard calibration curve of absorbance at 750 nm against the IR-783 concentration was made in aqueous solution. Next, all the s-SiO₂@PDA/IR-783 NPs centrifugation supernatants were collected, and the supernatant IR-783 concentration was calculated by measuring the absorbance based on the calibration curve drawn with standard IR-783 solutions. Then, the incorporation ratio of IR-783 into s-SiO₂@PDA NPs was determined based on the IR-783 concentration in the supernatant and the amount of IR-783 used in the synthesis of s-SiO₂@PDA/IR-783 NPs.

Fluorescence Imaging of COS-7 Cells. In this study, s-SiO₂@PDA/IR-783 NPs were introduced into the COS-7 cells (originally isolated from African green monkey kidney) by lipofectamine 2000, a cationic-lipid transfection reagent for cultured cell lines.^{10,41} The aqueous solution containing s-SiO₂@PDA/IR-783 NPs (0.15 mg mL⁻¹) was mixed with the same volume of lipofectamine aqueous solution and was vortexed vigorously. Then, the mixture was added directly to the culturing medium of COS-7 cells, which was Dulbecco's modified Eagle's medium with 10% fetal bovine serum. They were cultured at 37 °C under 5% humidified CO₂ for 20 h. After that, the COS-7 cells were washed with a PBS buffer aqueous solution to remove unincorporated s-SiO₂@PDA/IR-783 NPs. The images of the COS-7 cells were captured using a custom-built confocal fluorescence microscope.⁴⁴ The s-SiO₂@PDA/IR-783 NPs were excited at 685 nm (0.3 mW) using a HL6750MG semiconductor laser (Opnext, USA). Fluorescence emitted at wavelengths greater than 700 nm was integrated and digitized, with the signal shown in white color. As a control, the same experiment was conducted with IR-783 only, whose concentration was set to the same as that of the IR-783 concentration in the experiment of SiO₂@PDA/IR-783 NPs.

■ ASSOCIATED CONTENT

Supporting Information

The Supporting Information is available free of charge at <https://pubs.acs.org/doi/10.1021/acsomega.3c09655>.

Additional spectral data and images (PDF)

■ AUTHOR INFORMATION

Corresponding Author

Yoshio Nakahara – Faculty of Systems Engineering,
Wakayama University, Wakayama 640-8510, Japan;
✉ orcid.org/0000-0002-9850-8333; Email: nakahara@wakayama-u.ac.jp

Authors

Haruki Nakabayashi – Faculty of Systems Engineering,
Wakayama University, Wakayama 640-8510, Japan
Jun Miyazaki – Faculty of Systems Engineering, Wakayama
University, Wakayama 640-8510, Japan; ✉ orcid.org/0000-0002-9889-8888

Mitsuru Watanabe – Morinomiya Center, Osaka Research Institute of Industrial Science and Technology, Osaka 536-8553, Japan

Toshiyuki Tamai – Morinomiya Center, Osaka Research Institute of Industrial Science and Technology, Osaka 536-8553, Japan

Setsuko Yajima – Faculty of Systems Engineering, Wakayama University, Wakayama 640-8510, Japan; orcid.org/0000-0001-9644-0032

Complete contact information is available at:
<https://pubs.acs.org/10.1021/acsomega.3c09655>

Author Contributions

The manuscript was written through contributions of all authors. All authors have given approval to the final version of the manuscript. These authors contributed equally.

Notes

The authors declare no competing financial interest.

ACKNOWLEDGMENTS

This study was financially supported by a Grant-in-Aid for Scientific Research (C) under project numbers 20K05555 and 23K04809 from the Japan Society for the Promotion of Science (JSPS).

REFERENCES

- (1) Dayyani, N.; Khoei, S.; Ramazani, A. Design and synthesis of pH-sensitive polyamino-ester magneto-dendrimers: Surface functional groups effect on viability of human prostate carcinoma cell lines DU145. *Eur. J. Med. Chem.* **2015**, *98*, 190–202.
- (2) Motevalizadeh, S. F.; Khoobi, M.; Sadighi, A.; Khalilvand-Sedagheh, M.; Pazhouhandeh, M.; Ramazani, A.; Faramarzi, M. A.; Shafiee, A. Lipase immobilization onto polyethylenimine coated magnetic nanoparticles assisted by divalent metal chelated ions. *J. Mol. Catal. B Enzym.* **2015**, *120*, 75–83.
- (3) Tarasi, R.; Khoobi, M.; Niknejad, H.; Ramazani, A.; Ma'mani, L.; Bahadorikhalili, S.; Shafiee, A. β -cyclodextrin functionalized poly (5-amidiso-phthalic acid) grafted Fe_3O_4 magnetic nanoparticles: A novel biocompatible nanocomposite for targeted docetaxel delivery. *J. Magn. Mater.* **2016**, *417*, 451–459.
- (4) Gao, D.; Hu, D.; Liu, X.; Zhang, X.; Yuan, Z.; Sheng, Z.; Zheng, H. Recent Advances in Conjugated Polymer Nanoparticles for NIR-II Imaging and Therapy. *ACS Appl. Polym. Mater.* **2020**, *2*, 4241–4257.
- (5) Biffi, S.; Petrizza, L.; Rampazzo, E.; Voltan, R.; Sgarzi, M.; Garrovo, C.; Prodi, L.; Andolfi, L.; Agnoletto, C.; Zauli, G.; Secchiero, P. Multiple dye-doped NIR-emitting silica nanoparticles for both flow cytometry and in vivo imaging. *RSC Adv.* **2014**, *4*, 18278–18285.
- (6) Prodi, L.; Biffi, S.; Petrizza, L.; Garrovo, C.; Rampazzo, E.; Andolfi, L.; Giustetto, P.; Nikolov, I.; Kurdi, G.; Danailov, M.; Zauli, G.; Secchiero, P. Multimodal near-infrared-emitting PluS Silica nanoparticles with fluorescent, photoacoustic, and photothermal capabilities. *Int. J. Nanomed.* **2016**, *11*, 4865–4874.
- (7) Chen, J.; Luo, H.; Liu, Y.; Zhang, W.; Li, H.; Luo, T.; Zhang, K.; Zhao, Y.; Liu, J. Oxygen-Self-Produced Nanoplatfor for Relieving Hypoxia and Breaking Resistance to Sonodynamic Treatment of Pancreatic Cancer. *ACS Nano* **2017**, *11*, 12849–12862.
- (8) Rampazzo, E.; Genovese, D.; Palomba, F.; Prodi, L.; Zaccheroni, N. NIR-fluorescent dye doped silica nanoparticles for in vivo imaging, sensing and theranostic. *Methods Appl. Fluoresc.* **2018**, *6*, 022002.
- (9) Jiao, L.; Liu, Y.; Zhang, X.; Hong, G.; Zheng, J.; Cui, J.; Peng, X.; Song, F. Constructing a Local Hydrophobic Cage in Dye-Doped Fluorescent Silica Nanoparticles to Enhance the Photophysical Properties. *ACS Cent. Sci.* **2020**, *6*, 747–759.
- (10) Nakahara, Y.; Nakajima, Y.; Okada, S.; Miyazaki, J.; Yajima, S. Synthesis of Silica Nanoparticles with Physical Encapsulation of Near-Infrared Fluorescent Dyes and Their Tannic Acid Coating. *ACS Omega* **2021**, *6*, 17651–17659.
- (11) Gubala, V.; Giovannini, G.; Kunc, F.; Monopoli, M. P.; Moore, C. J. Dye-Doped Silica Nanoparticles: Synthesis, Surface Chemistry and Bioapplications. *Cancer Nanotechnol.* **2020**, *11*, 1–43.
- (12) Lian, Y.; Ding, L.-J.; Zhang, W.; Zhang, X.-A.; Zhang, Y.-L.; Lin, Z.-Z.; Wang, X.-D. Synthesis of highly stable cyanine-dye-doped silica nanoparticle for biological applications. *Methods Appl. Fluoresc.* **2018**, *6*, 034002.
- (13) Jin, A.; Wang, Y.; Lin, K.; Jiang, L. Nanoparticles modified by polydopamine: Working as “drug” carriers. *Bioact. Mater.* **2020**, *5*, 522–541.
- (14) Lee, H.; Dellatore, S. M.; Miller, W. M.; Messersmith, P. B. Mussel-Inspired Surface Chemistry for Multifunctional Coatings. *Science* **2007**, *318*, 426–430.
- (15) Lu, J.; Cai, L.; Dai, Y.; Liu, Y.; Zuo, F.; Ni, C.; Shi, M.; Li, J. Polydopamine-Based Nanoparticles for Photothermal Therapy/Chemotherapy and their Synergistic Therapy with Autophagy Inhibitor to Promote Antitumor Treatment. *Chem. Rec.* **2021**, *21*, 781–796.
- (16) Cheng, Y.; Zhang, S.; Kang, N.; Huang, J.; Lv, X.; Wen, K.; Ye, S.; Chen, Z.; Zhou, X.; Ren, L. Polydopamine-Coated Manganese Carbonate Nanoparticles for Amplified Magnetic Resonance Imaging-Guided Photothermal Therapy. *ACS Appl. Mater. Interfaces* **2017**, *9*, 19296–19306.
- (17) Cheng, W.; Liang, C.; Xu, L.; Liu, G.; Gao, N.; Tao, W.; Luo, L.; Zuo, Y.; Wang, X.; Zhang, X.; Zeng, X.; Mei, L. TPGS-Functionalized Polydopamine-Modified Mesoporous Silica as Drug Nanocarriers for Enhanced Lung Cancer Chemotherapy against Multidrug Resistance. *Small* **2017**, *13*, 1700623.
- (18) Dong, Z.; Gong, H.; Gao, M.; Zhu, W.; Sun, X.; Feng, L.; Fu, T.; Li, Y.; Liu, Z. Polydopamine Nanoparticles as a Versatile Molecular Loading Platform to Enable Imaging-guided Cancer Combination Therapy. *Theranostics* **2016**, *6*, 1031–1042.
- (19) Sun, L.; Li, Q.; Zhang, L.; Xu, Z.; Kang, Y.; Xue, P. PEGylated Polydopamine Nanoparticles Incorporated with Indocyanine Green and Doxorubicin for Magnetically Guided Multimodal Cancer Therapy Triggered by Near-Infrared Light. *ACS Appl. Nano Mater.* **2018**, *1*, 325–336.
- (20) Wang, S.; Zhao, X.; Wang, S.; Qian, J.; He, S. Biologically Inspired Polydopamine Capped Gold Nanorods for Drug Delivery and Light-Mediated Cancer Therapy. *ACS Appl. Mater. Interfaces* **2016**, *8*, 24368–24384.
- (21) Wei, J.; Wu, C.; Wu, X.; Wu, L. A sensitive electrochemical bisphenol A sensor based on molecularly imprinted polydopamine-coated Fe_3O_4 microspheres. *Anal. Sci.* **2022**, *38*, 339–346.
- (22) Liu, B.; Li, C.; Xing, B.; Yang, P.; Lin, J. Multifunctional UCNPs@PDA-ICG nanocomposites for upconversion imaging and combined photothermal/photodynamic therapy with enhanced antitumor efficacy. *J. Mater. Chem. B* **2016**, *4*, 4884–4894.
- (23) Hu, D.; Liu, C.; Song, L.; Cui, H.; Gao, G.; Liu, P.; Sheng, Z.; Cai, L. Indocyanine green-loaded polydopamine-iron ions coordination nanoparticles for photoacoustic/magnetic resonance dual-modal imaging-guided cancer photothermal therapy. *Nanoscale* **2016**, *8*, 17150–17158.
- (24) Sheng, Z.; Hu, D.; Xue, M.; He, M.; Gong, P.; Cai, L. Indocyanine Green Nanoparticles for Theranostic Applications. *Nano-Micro Lett.* **2013**, *5*, 145–150.
- (25) Quan, B.; Choi, K.; Kim, Y.-H.; Kang, K. W.; Chung, D. S. Near infrared dye indocyanine green doped silica nanoparticles for biological imaging. *Talanta* **2012**, *99*, 387–393.
- (26) Huang, C.; Zhang, Z.; Guo, Q.; Zhang, L.; Fan, F.; Qin, Y.; Wang, H.; Zhou, S.; Ou-Yang, W.; Sun, H.; Leng, X.; Pan, X.; Kong, D.; Zhang, L.; Zhu, D. A Dual-Model Imaging Theragnostic System Based on Mesoporous Silica Nanoparticles for Enhanced Cancer Phototherapy. *Adv. Healthcare Mater.* **2019**, *8*, 1900840.
- (27) Song, J. T.; Yang, X. Q.; Zhang, X. S.; Yan, D. M.; Wang, Z. Y.; Zhao, Y. D. Facile Synthesis of Gold Nanospheres Modified by Positively Charged Mesoporous Silica, Loaded with Near-Infrared

Fluorescent Dye, for in Vivo X-ray Computed Tomography and Fluorescence Dual Mode Imaging. *ACS Appl. Mater. Interfaces* **2015**, *7*, 17287–17297.

(28) Harrison, V. S. R.; Carney, C. E.; MacRenaris, K. W.; Waters, E. A.; Meade, T. J. Multimeric Near IR-MR Contrast Agent for Multimodal In Vivo Imaging. *J. Am. Chem. Soc.* **2015**, *137*, 9108–9116.

(29) McNeil, S. E. Nanoparticle Therapeutics: a Personal Perspective. *Wiley Interdiscip. Rev.: Nanomed. Nanobiotechnol.* **2009**, *1*, 264–271.

(30) Xu, S.; Hartvickson, S.; Zhao, J. X.; Huang, J.; Lv, X.; Wen, K.; Ye, S.; Chen, Z.; Zhou, X.; Ren, L. Increasing Surface Area of Silica Nanoparticles with a Rough Surface. *ACS Appl. Mater. Interfaces* **2011**, *3*, 1865–1872.

(31) Maziukiewicz, D.; Grzeskowiak, B. F.; Coy, E.; Jurga, S.; Mrowczynski, R. NDs@PDA@ICG Conjugates for Photothermal Therapy of Glioblastoma Multiforme. *Biomimetics* **2019**, *4*, 3–17.

(32) Schneider, C. A.; Rasband, W. S.; Eliceiri, K. W. NIH Image to ImageJ: 25 years of image analysis. *Nat. Methods* **2012**, *9*, 671–675.

(33) Paci, J. T.; Man, H. B.; Saha, B.; Ho, D.; Schatz, G. C. Understanding the surfaces of nanodiamonds. *J. Phys. Chem. C* **2013**, *117*, 17256–17267.

(34) Abouelmagd, S. A.; Meng, F.; Kim, B.-K.; Hyun, H.; Yeo, Y. Tannic Acid-Mediated Surface Functionalization of Polymeric Nanoparticles. *ACS Biomater. Sci. Eng.* **2016**, *2*, 2294–2303.

(35) Su, Y.; Liu, Y.; Xu, X.; Zhou, J.; Xu, L.; Xu, X.; Wang, D.; Li, M.; Chen, K.; Wang, W. On-Demand Versatile Prodrug Nanomicelle for Tumor-Specific Bioimaging and Photothermal-Chemo Synergistic Cancer Therapy. *ACS Appl. Mater. Interfaces* **2018**, *10*, 38700–38714.

(36) Yang, X.; Shi, C.; Tong, R.; Qian, W.; Zhou, H. E.; Wang, R.; Zhu, G.; Cheng, J.; Yang, V. W.; Cheng, T.; Henary, M.; Strekowski, L.; Chung, L. W. K. Near IR Heptamethine Cyanine Dye-Mediated Cancer Imaging. *Clin. Cancer Res.* **2010**, *16*, 2833–2844.

(37) Huang, X.; Wu, J.; He, M.; Hou, X.; Wang, Y.; Cai, X.; Xin, H.; Gao, F.; Chen, Y. Combined Cancer Chemo-Photodynamic and Photothermal Therapy Based on ICG/PDA/TPZ-Loaded Nanoparticles. *Mol. Pharm.* **2019**, *16*, 2172–2183.

(38) Yoo, J.; Won, Y.-Y. Phenomenology of the Initial Burst Release of Drugs from PLGA Microparticles. *ACS Biomater. Sci. Eng.* **2020**, *6*, 6053–6062.

(39) Zheng, M.; Yue, C.; Ma, Y.; Gong, P.; Zhao, P.; Zheng, C.; Sheng, Z.; Zhang, P.; Wang, Z.; Cai, L. Single-Step Assembly of DOX/ICG Loaded Lipid-Polymer Nanoparticles for Highly Effective Chemo-photothermal Combination Therapy. *ACS Nano* **2013**, *7*, 2056–2067.

(40) Clements, B. A.; Incani, V.; Kucharski, C.; Lavanifanar, A.; Ritchie, B.; Uludag, H. A comparative evaluation of poly-l-lysine-palmitic acid and Lipofectamine 2000 for plasmid delivery to bone marrow stromal cells. *Biomaterials* **2007**, *28*, 4693–4704.

(41) Nakahara, Y.; Tatsumi, Y.; Akimoto, I.; Osaki, S.; Doi, M.; Kimura, K. Fluorescent silica nanoparticles modified chemically with terbium complexes as potential bioimaging probes: their fluorescence and colloidal properties in water. *New J. Chem.* **2015**, *39*, 1452–1458.

(42) Yu, B.; Zhang, Y.; Zheng, W.; Fan, C.; Chen, T. Positive Surface Charge Enhances Selective Cellular Uptake and Anticancer Efficacy of Selenium Nanoparticles. *Inorg. Chem.* **2012**, *51*, 8956–8963.

(43) He, C. B.; Hu, Y. P.; Yin, L. C.; Tang, C.; Yin, C. H. Effects of Particle Size and Surface Charge on Cellular Uptake and Biodistribution of Polymeric Nanoparticles. *Biomaterials* **2010**, *31*, 3657–3666.

(44) Miyazaki, J.; Iida, T.; Tanaka, S.; Hayashi-Takagi, A.; Kasai, H.; Okabe, S.; Kobayashi, T. Fast 3D visualization of endogenous brain signals with high-sensitivity laser scanning photothermal microscopy. *Biomed. Opt. Express* **2016**, *7*, 1702–1710.